JEVT 17-0124 *Experimental Investigation*

Use of Synchrotron Radiation to Accurately Assess Cross-Sectional Area Reduction of the Aortic Branch Ostia Caused by Suprarenal Stent Wires

Zhonghua Sun, PhD[1] and Curtise K. C. Ng, PhD[1]

[1]Department of Medical Radiation Sciences, Curtin University, Perth, WA, Australia

Corresponding Author:
Professor Zhonghua Sun, Department of Medical Radiation Sciences, School of Science, Curtin University, GPO Box U1987, Perth, Western Australia 6845, Australia. Email: z.sun@curtin.edu.au

Abstract

Purpose: To compare in vivo the use of synchrotron radiation to computed tomography angiography (CTA) for the measurement of cross-sectional area (CSA) reduction of the aortic branch ostia caused by suprarenal stent-graft wires.

Methods: This study was performed with a Zenith stent-graft placed in a phantom of the human aorta to simulate treatment of abdominal aortic aneurysm. Synchrotron radiation scans were performed using beam energies between 40 and 100 keV and spatial resolution of 19.88 μm per pixel. CSA reduction of the aortic branch ostia by suprarenal stent wires was calculated based on these exposure factors and compared with measurements from CTA images acquired on a 64-row scanner with slice thicknesses of 1.0, 1.5, and 2.0 mm.

Results: Images acquired with synchrotron radiation showed <10% of the CSA occupied by stent wires when a single wire crossed a renal artery ostium and <20% for 2 wires crossing a renovisceral branch ostium. The corresponding areas ranged from 24% to 25% for a single wire and from 40% to 48% for double wires crossing the branch ostia when measured on CT images. The stent wire was accurately assessed on synchrotron radiation with a diameter between 0.38±0.01 mm and 0.53±0.03 mm, which is close to the actual size of 0.47±0.01 mm. The wire diameter measured on CT images was greatly overestimated (1.15±0.01 mm to 1.57±0.02 mm).

Conclusion: CTA has inferior spatial resolution that hinders accurate assessment of CSA reduction. This experiment demonstrated the superiority of synchrotron radiation over CTA for more accurate assessment of aortic stent wires and CSA reduction of the aortic branch ostia.

Keywords

abdominal aortic aneurysm, aorta, branch ostia, cross-sectional area, computed tomography, renal artery, superior mesenteric artery, synchrotron radiation, stent-graft, suprarenal stent wire

Introduction

Endovascular aneurysm repair (EVAR) has been increasingly used for treatment of patients with abdominal aortic aneurysm (AAA) due to the lower invasiveness and perioperative mortality compared to open surgery.[1-4] EVAR is a widely used technique in many clinical centers, with technical developments in aortic stent-grafts promoting its application to patients with complex AAA.[5] While many studies have reported satisfactory results of this less invasive procedure, the long-term outcomes of EVAR, specifically, the effect of aortic stent wires on renal blood flow and subsequent renal function is still a main concern to clinicians when evaluating the durability of this technique.[6-10]

AAA patients treated with EVAR have regular imaging surveillance to determine whether the aortic aneurysm is successfully excluded, the stent-graft is position properly in relation to the aortic branches, and the renovisceral arteries are patent. Computed tomography angiography (CTA) is currently the reference imaging modality for follow-up of EVAR.[11-15] Modern multidetector computed tomography (CT) scanners allow excellent assessment of changes in aneurysm morphology and configuration of the implanted stent-grafts.[16-18] However, the spatial resolution of the latest CT scanners, which have the isotropic voxel size of 0.4×0.4x0.4 mm^3, is still suboptimal for the visualization of the stent wires because, according to our previous studies,[19-21] the wire diameter is overestimated on CTA images by from 1.0 mm to 2.0 mm. This makes the stent wires look much thicker than the actual size, which is <0.5 mm. Thus, the cross-sectional area (CSA) of the branch ostia is exaggerated when calculated based on the wire thickness measured on CT images.[19] This limitation could be addressed by synchrotron radiation, which has a spatial resolution between 10 and 20 μm, >10-fold higher than the latest multidetector CT scanners (300–400 μm).

There have been many applications of synchrotron radiation in various areas, including the investigation of cardiovascular disease.[22-26] Studies have shown that synchrotron radiation accurately captures the mechanical structure of coronary stents and atherosclerotic plaques, as well as components of

calcified lesions. Our recent experience using synchrotron radiation in an aortic phantom study demonstrated the advantage of this technique in the visualization of aortic stent wires when compared to CT imaging.[27] This study further expands the application of synchrotron radiation in aortic stent-grafting by examining the hypothesis that synchrotron radiation allows more accurate assessment of CSA reduction of branch ostia when compared to the commonly used multidetector CT imaging technique.

Methods

Phantom

A phantom of the human aorta was developed previously[19-21] using a rapid prototyping technique. These studies demonstrated the accuracy of the phantom to replicate diameters of the aorta and its main branches and determined the optimal CT scanning protocols. The current study used the same phantom because it allows visualization and comparison of the renal arteries, superior mesenteric artery, (SMA), and AAA between synchrotron radiation and CT scans (Figure 1).

Aortic Stent-Graft

Similar to our previous reports, a commercially available endovascular stent-graft (Zenith AAA; William Cook Europe, Bjaeverskov, Denmark) was used to simulate AAA treatment. The Zenith stent-graft has an uncovered suprarenal component that consists of a number of bare metal stent wires (Figure 2), thus allowing it to be deployed above the renal arteries without compromising blood flow to the kidneys. The suprarenal stent wire measured 0.47±0.01 mm according to a digital caliper.

Experimental Setup of Synchrotron Tomography

Synchrotron radiation (tomography) scans were acquired on the Imaging and Medical Beamline (IMBL) at the Australian Synchrotron Facility in Melbourne,

Australia. The IMBL uses monochromatic x-rays from a synchrotron source to produce high-resolution images with contrast and content details far superior to those acquired with CT and other imaging techniques. Therefore, no contrast medium was used in these experiments. The synchrotron radiation images were recorded on detectors with a 70×20-mm field of view with a pixel size of 19.88 μm. Details of the experimental setup on IMBL have been described previously.[27] In brief, synchrotron radiation scans were performed with a range of beam energies from 40 to 100 keV in 10-keV increments to examine the effects on visualization of stent wires across the branch ostia and measurement of CSA coverage.

CT Scanning Techniques

In our previous experiments, a series of CT scans were tested on the phantom using a 64-row CT scanner (Siemens Definition; Siemens Healthcare, Forchheim, Germany) with different protocols covering a range of slice thicknesses and pitch values. A CT scanning protocol consisting of 1.5-mm slice thickness and 1.5 pitch, with 100 kV and 180 mAs was found to be optimal according to quantitative assessment of image quality based on 2-dimensional (2D) and 3-dimensional (3D) images, with significant reduction in radiation dose.[28] Thus, in this study, CT images were acquired with slice thicknesses of 1.0, 1.5, and 2.0 mm, a pitch of 1.5, and exposure factors of 100 kV and 180 mAs for comparison with synchrotron radiation images as regards stent wire thickness and CSA reduction of the branch ostia. The CT dose index volume and dose length product for these CT protocols were 7.60, 7.60, and 7.60 mGy and 133, 125, and 136 mGy·cm, respectively, resulting in corresponding effective doses of 2.00, 1.88, and 2.04 mSv.

Image Processing and Measurements

Synchrotron radiation images in tagged image file format and 64-slice CT images in Digital Imaging and Communications in Medicine format were transferred to a separate workstation equipped with Analyze (version 12.0;

AnalyzeDirect, Inc., Lexana, KS, USA) for image processing and measurement. Details of measurements of the stent wire diameter were well described previously in our study of synchrotron radiation images based on 2D and 3D reconstructed images.[27]

According to previous reports,[19,21] suprarenal stent wires can assume 4 different configurations in relation to the renal and SMA ostia: single wire on center, single wire off center, 2 wires off center, and 2 wires in a V shape. Our previous study confirmed that ostial CSA reduction was determined by the diameter and number of stent wires crossing the ostium,[19] so only 2 stent wire configurations were tested. Thus, the stent-graft was placed inside the phantom such that a single wire crossed the left renal ostium peripherally (off-center wire) and 2 stent wires crossed the right renal and SMA ostia peripherally (Figure 1A). The central single wire and dual V-shaped wires were not included.

The CSA occupied by the stent wire/wires was calculated according to Liffman et al, [29] who proposed formulas that take into account the diameter of the stent wire and distance of the wire to the central axis of the branch ostium. Measurements of wire diameter and distance were performed on 3D virtual intravascular endoscopy (VIE) images, which provide unique intravascular views of the 3D relationship between the branch ostia and stent wires (Figures 3 and 4), as explained previously.[20,21,29] In brief, a thresholding technique was used to generate VIE images of aortic stent wires with measurements performed 3 times at each anatomical location. A mean value was taken to avoid intraobserver disagreement. Selection of an appropriate threshold is dependent on clearly visualizing the aortic stent wires without fragmented or discontinuous appearances on VIE.[21]

Statistical Analysis

Continuous variables were presented as the mean ± standard deviation. Mean values of stent wire thickness and CSA occupied by stent wires measured on synchrotron radiation and CT images were compared using the Student *t* test; $p<0.05$ was considered statistically significant. Statistical analyses were

performed using SPSS software (version 24.0; IBM Corporation, Armonk, NY, USA).

Results

The stent wire diameter was more accurately assessed on images acquired with synchrotron radiation (Figure 5A), with measured thicknesses of 0.38±0.01 mm to 0.53±0.03 mm, close to the actual size of wire diameter of the aortic stent-graft (0.47±0.01 mm). Table 1 shows measurements of stent wire diameters at various anatomical locations with different scanning protocols. The 40-keV protocol for synchrotron radiation resulted in more distorted wire diameters at all 3 branch ostia than other protocols ($p<0.05$), indicating inferior visualization or inaccurate assessment because of low energy effect. In contrast, the wire diameter was overestimated on CT images (Table 2), with measured thicknesses ranging from 1.15±0.01 mm to 1.57±0.02 mm, which makes it look like much thicker than the real size.

The key findings of this study lie in more accurate calculation of the CSA occupied by stent wires through the use of synchrotron radiation compared to CT images. Table 1 shows calculated ostial CSA coverage for wires in different configurations. The results showed <10% CSA coverage of the left renal artery ostium when it was crossed by a single stent wire and <20% coverage of the right renal and SMA ostia when crossed by 2 stent wires. The CSA coverage by stent wires was significantly increased when assessed on CT images ($p<0.001$), with covered areas of 24% to 25%, 44% to 48%, and 40% to 43%, corresponding to the left renal, right renal, and SMA ostia, respectively. This is mainly because of the overestimated wire thickness on CT images.

Discussion

Our findings reveal the superior accuracy of suprarenal stent wire imaging using ultra-high-resolution synchrotron radiation compared to the conventional CT images. The aortic stent wires can be accurately measured on images acquired

with synchrotron radiation, with diameters similar to the actual size, thus allowing determination of the CSA reduction of the branch ostia by stent wires. This has significant clinical impact because the potential effects of suprarenal stent wires on renal perfusion can now be measured with a precision heretofore unobtainable. Knowing the exact extent of wire coverage could uncover a risk for thrombus formation or implantation-induced stenosis.

Technological developments in aortic stent-grafts have overcome limitations of previous products and now accommodate a wider range of indications.[30] However, alteration of the hemodynamic environment associated with these stent-grafts remains a hot topic in the literature. The deployment of endovascular devices in the abdominal aorta alters the local hemodynamics, thus promoting thrombus formation in the stent-graft. Our previous study and others using computational fluid dynamics in idealized or patient-specific models did not show significant impact of suprarenal stent wires on renal hemodynamic changes, with <5% flow velocity reduction in different types or configurations of stent wires crossing the renal ostium.[29,31] Nevertheless, reduction of flow velocity was increased to as much as 40% when the stent wire diameter was increased from 0.4 to 1.0 or 2.0 mm due to material buildup (neointimal hyperplasia) on the stent surface. This may lead to stent-graft–induced stenosis because of disturbed flow or thrombus accumulation on the stent-graft/stent wire surface,[31] although this needs to be verified by clinical studies with longer follow-up.

Several studies have reported thrombus formation in AAA stent-grafts,[32-36] with an incidence ranging from 15% to 33% depending on the devices used. Although these thrombotic deposits did not cause atheroembolic events, formation of thrombus on the stent wire surface could further increase renal ostial CSA reduction, which may compromise blood flow to the renal arteries. Thrombus formation in the stent-graft is a common phenomenon, and its significance remains unclear. However, Wu et al[37] showed a significant correlation between deposition of thrombus and the ratio of the CSA of the main stent-graft to the iliac limbs ($p=0.04$) and length of the main body ($p=0.01$).

Therefore, the presence of thrombotic materials in the stent wires should not be ignored due to the potential risk of affecting renal perfusion. This could be further studied with synchrotron radiation in animal experiments. Some recent studies on mice have demonstrated the accuracy of synchrotron radiation for 3D morphological assessment of the cardiovascular system, ranging from large vascular structures to microscopic details of atherosclerotic plaques.[38-40]

Results of our study further advance our understanding of the effect of stent wires on renal and other branch ostia in terms of CSA reduction. There are very limited studies available in the literature on the CSA coverage by stent wires,[19] as most of the research focuses on CT follow-up of aneurysm remodeling in terms of aneurysm size change or CSA reduction of the aneurysms.[41-43] Given the above-mentioned possibilities of thrombus formation and hemodynamic changes by the stent-graft / stent wires, synchrotron radiation offers a novel technique for accurate assessment of ostial CSA reduction by stent wires.

Although synchrotron radiation has been proven to be a safe imaging modality in the diagnosis of cardiovascular disease,[26] it is not recommended as a routine technique for EVAR surveillance because it mainly serves as a research tool. Currently, CTA is the preferred imaging modality in AAA diagnosis and EVAR follow-up. However, repeated CT scans expose patients to high cumulative radiation doses and nephrotoxic intravenous contrast medium.[44,45] This has raised serious concerns. To address this issue, low-dose CTA protocols have been reported to show the feasibility of reducing both radiation dose (reduce tube voltage from 120 to 100 or 80 kV) and contrast volume (lower contrast medium to 30 mL) while capturing diagnostic-quality images.[46-48]

Another strategy to solve this issue is to use duplex ultrasound as an alternative to CTA in the follow-up of EVAR patients. Several authors have shown that contrast-enhanced ultrasound is as accurate as or better than CTA in detecting endoleaks, monitoring aneurysm dimensional changes, and assessing stented vessel patency by analyzing hemodynamic flow to the renal arteries.[49-51]

A recent study[52] advocated increasing the use of ultrasound while reducing the use of CT to reduce costs and radiation dose.

Limitations

First, contrast medium was not used in our phantom experiments because of the superior spatial and contrast resolution of synchrotron radiation. Further, any scatter artifacts or contrast decrease that might arise from a patient could not be assessed in this phantom study.

Second, CT images in this study were acquired on a 64-row scanner, which is widely available in many clinical centers, although it does not represent the latest CT models. Despite the limitation of a 1-mm slice thickness used in this study, thin slice images, such as 0.5 or 0.625 mm, still resulted in overestimation of wire thickness, even with the generation of isotropic volume data (Figure 6). High-resolution CT with a spatial resolution of 0.23 mm shows improved diagnostic performance as opposed to the 0.5 to 0.625-mm spatial resolution of the standard 64-row scanner, thus it may allow better visualization of stent wires.[53]

Third, although the hollow phantom used in this study has anatomical details representing realistic aortic structures, the phantom wall seems to be quite thick. With currently available 3D printing techniques, a more realistic patient-specific 3D printed model would be desirable to replicate both anatomy and pathology for experimental studies.[54-56]

Fourth, radiation dose associated with synchrotron radiation was not measured in this study as our focus was to determine the stent wire thickness in relation to CSA reduction. Further experiments with measurement of radiation exposure due to synchrotron radiation are needed to enable comparison of radiation dose between synchrotron radiation and conventional CT imaging.

Finally, only the Zenith stent-graft was tested in this study. Currently, there are different types of stent-grafts available for treatment of AAA, and most importantly, the development of thrombus in stent-grafts depends on the type of devices used.[32] Thus, it is necessary to conduct further research with different

aortic stent-graft models to verify our findings with regard to the best imaging technique to accurately identify ostial CSA reduction by stent wires.

Conclusion

Compared to CT scanning, high-resolution synchrotron radiation can more precisely image suprarenal stent wires crossing aortic branch ostia, thus assisting accurate study of ostial CSA reduction in patients treated with aortic stent-grafts.

Acknowledgments

Authors would like to thank Dr. Chris Hall from Australian Synchrotron for his advice and assistance in our experiments. We thank Mr. Zhiyue Sun for his assistance in the data analysis. This research was undertaken on the Imaging and Medical Beamline at the Australian Synchrotron, Victoria, Australia.

Declaration of Conflicting Interests

The author(s) declare no potential conflicts of interest with respect to the research, authorship, and/or publication of this article.

Funding

The author(s) received no financial support for the research, authorship, and/or publication of this article.

References

1. Greenhalgh RM, Brown LC, Kwong GP, et al. Comparison of endovascular aneurysm repair with open repair in patients with abdominal aortic aneurysm (EVAR trial 1), 30-day operative mortality results: randomised controlled trial. *Lancet*. 2004;364:843-848.
2. Prinssen M, Verhoeven EL, Buth J, et al. A randomized trial comparing conventional and endovascular repair of abdominal aortic aneurysms. *N Engl J Med*. 2004;351:1607-1618.
3. Harris PL, Vallabhaneni SR, Desgranges P, et al. Incidence and risk factors of late rupture, conversion, and death after endovascular repair of infrarenal aortic aneurysms: the EUROSTAR experience. *J Vasc Surg*. 2000;32:739-749.
4. Brown LC, Greenhalgh RM, Thompson SG, et al. Does EVAR alter the rate of cardiovascular events in patients with abdominal aortic aneurysm considered unfit for open repair? Results from the randomised EVAR trial 2. *Eur J Vasc Endovasc Surg*. 2010;39:396-402.
5. Bicknell CD, Cheshire NJ, Riga CV, et al. Treatment of complex aneurysmal disease with fenestrated and branched stent grafts. *Eur J Vasc Endovasc Surg*. 2009;37:175-181.
6. O'Donnell ME, Sun Z, Winder EJ, et al. Suprarenal fixation of endovascular aortic stent grafts: assessment of medium-term to long-term renal function by analysis of juxtarenal stent morphology. *J Vasc Surg*. 2007;45:694-700.
7. Greenberg RK, Chuter TA, Lawrence-Brown M, et al. Analysis of renal function after aneurysm repair with a device using suprarenal fixation (Zenith AAA Endovascular Graft) in contrast to open surgical repair. *J Vasc Surg*. 2004;39:1219-1228.
8. Saratzis AN, Bath MF, Harrison SC, et al. Impact of fenestrated endovascular abdominal aortic aneurysm repair on renal function. *J Endovasc Ther.* 2015;22:889-896.

9. Sun Z, Mwipatayi BP, Semmens JB, et al. Short to midterm outcomes of fenestrated endovascular grafts in the treatment of abdominal aortic aneurysms: a systematic review. *J Endovasc Ther.* 2006;13:747-753.
10. Zarkowsky DS, Hicks CW, Bostock IC, et al. Renal dysfunction and the associated decrease in survival after elective endovascular aneurysm repair. *J Vasc Surg*. 2016;64:1278-1285.
11. Sun Z, O'Donnell M, Winder R, et al. Effect of suprarenal fixation of aortic stent-grafts on renal ostium: Assessment of morphological changes by virtual intravascular endoscopy. *J Endovasc Ther*. 2007;14:650-660.
12. Sun Z. Helical CT angiography of abdominal aortic aneurysms treated with suprarenal stent-grafting. *Cardiovasc Intervent Radiol*. 2003;26:290-295.
13. Rydberg J, Kopecky KK, Lalka SG, et al. Stent grafting of abdominal aortic aneurysms: Pre- and postoperative evaluation with multislice helical CT. *J Comput Assist Tomogr*. 2001;25:580-586.
14. Rozenblit A, Patlas M, Rosenbaum AT, et al. Detection of endoleaks after endovascular repair of abdominal aortic aneurysm repair: value of unenhanced and delayed helical CT acquisitions. *Radiology*. 2003;227:426-433.
15. Stavropoulos SW, Clark TW, Carpenter JP, et al. Use of CT angiography to classify endoleaks after endovascular repair of abdominal aortic aneurysms. *J Vasc Interv Radiol*. 2005;16 663-667.
16. Sun Z, Choo GH, Ng KH. Coronary CT angiography: current status and continuing challenges. *Br J Radiol.* 2012;85:495-510.
17. Sun Z, Almoudi M, Cao Y. CT angiography in the diagnosis of cardiovascular disease: A transformation in cardiovascular CT practice. *Quant Imaging Med Surg*. 2014;4:376-396.
18. Tan SK, Yeong CH, Ng KH, et al. Recent update on radiation dose assessment for the state-of-art coronary computed tomography angiography (CCTA) protocols. *Plos One*. 2016;11:e0161543.

19. Sun Z, Zheng H. Cross-sectional area reduction of the renal ostium by suprarenal stent wires: in vitro phantom study by CT virtual angioscopy. *Comput Med Imaging Graph*. 2004;28:345-351.
20. Sun Z, Winder JR, Kelly BE, et al. Assessment of VIE image quality using helical CT angiography: in vitro phantom study. *Comput Med Imaging Graph*. 2004;28:3-12.
21. Sun Z, Gallagher E. Multislice CT virtual intravascular endoscopy for abdominal aortic aneurysm stent-grafts. *J Vasc Interv Radiol*. 2004;15:961-970.
22. Lewis R. Medical applications of synchrotron radiation x-rays. *Phys Med Biol*. 1997;42:1213-1243.
23. Sun Z. The promise of synchrotron radiation in medical science. *Australasian Med J*. 2009;1:1-5.
24. Connolley T, Nash D, Buffiere JY, et al. X-ray micro-tomography of a coronary stent deployed in a model artery. *Med Eng Phys*. 2007;29:1132-1141.
25. Wix WR, Kupper W, Dill T, et al. Comparison of intravenous coronary angiography using synchrotron radiation with selective coronary angiography. *J Synchrotron Radiat*. 2003;10:219-227.
26. Bertrand B, Esteve F, Elleaume H, et al. Comparison of synchrotron radiation angiography with conventional angiography for the diagnosis of in-stent restenosis after percutaneous transluminal coronary angioplasty. *Eur Heart J.* 2005;26:1284-1291.
27. Sun Z, Ng CK. Synchrotron radiation imaging of aortic stent-grafting: An in vitro phantom study. *J Med Imaging Health Informatics*. 2017;7:890-896.
28. Sun Z, Ng C. Dual source CT angiography in aortic stent-grafting: An in vitro aorta phantom study of image noise and radiation dose. *Acad Radiol*. 2010;17:884-893.
29. Liffman K, Lawrence-Brown MM, Semmens JB, et al. Suprarenal fixation: Effect on blood flow of an endoluminal stent wire across an arterial orifice. *J Endovasc Ther*. 2003;10:260-274.

30. de Donato G, Setacci F, Bresadola L, et al; TriVascular Ovation Italian Study (TOIS) Collaborators. Midterm results of proximal aneurysm sealing with the Ovation stent-graft according to on- vs off-label use. *J Endovasc Ther.* 2017;24:191-197.
31. Sun Z, Chaichana T. Investigation of hemodynamic effect of stent wires on renal arteries in patients with abdominal aortic aneurysms treated with suprarenal stent-grafts. *Cardiovasc Intervent Radiol*. 2009;32:647-657.
32. Aristokleous N, Kontopodis NG, Tzirakis K, et al. Hemodynamic impact of abdominal aortic aneurysm stent-graft implantation-induced stenosis. *Med Bio Eng Comput*. 2015;54:1523-1532.
33. Maleux G, Koolen M, Heye S, et al. Mural thrombotic deposits in abdominal aortic endografts are common and do not require additional treatment at short-term and midterm follow-up. *J Vasc Interv Radiol*. 2008;19:1558-1562.
34. Wegener M, Gorich J, Kramer S, et al. Thrombus formation in aortic endografts. *J Endovasc Ther*. 2001;8:372-379.
35. Shin IS, Kim JM, Kim KL, et al. Early growth response factor-1 is associated with intraluminal thrombus formation in human abdominal aortic aneurysm. *J Am Coll Cardiol*. 2009;53:792-799.
36. Aho PS, Niemi T, Piilonen A, et al. Interplay between coagulation and inflammation in open and endovascular abdominal aortic aneurysm repair impact of intra-aneurysmal thrombus. *Scand J Surg*. 2007;96:229-235.
37. Wu IH, Liang PC, Huang SC, et al. The significance of endograft geometry on the incidence of intraprosthetic thrombus deposits after abdominal endovascular grafting. *Eur J Vasc Endovasc Surg*. 2009;38:741-747.
38. Bonanno G, Coppo S, Modregger P, et al. Ultra-high-resolution 3D imaging of atherosclerotic in mice with synchrotron differential phase contrast: a proof of concept study. *Sci Rep*. 2015;5:11980.
39. Zhang MQ, Zhou L, Deng QF, et al. Ultra-high-resolution 3D digitalized imaging of the cerebral angioarchitecture in rats using synchrotron radiation. *Sci Rep*. 2015;5:14982.

40. Li R, Wang D, Sun C, et al. Towards automated quantitative vasculature understanding via ultra high-resolution imagery. *Adv Exp Med Biol*. 2015;823:177-189.
41. Martufi G, Lindquist Liljeqvist M, Sakalihasan N, et al. Local diameter, wall stress, and thrombus thickness influence the local growth of abdominal aortic aneurysms. *J Endovasc Ther*. 2016;23:957-966.
42. Martufi G, Auer M, Roy J, et al. Multidimensional growth measurements abdominal aortic aneurysms. *J Vasc Surg*. 2013;58:748-755.
43. Nowicka M, Kowalczyk A, Rusak G, et al. Evaluation the aortic aneurysm remodeling after a successful stentgraft implantation. *Pol J Radiol*. 2016;81:486-490.
44. de Ruiter QM, Reitsma JB, Moll FL, et al. Meta-analysis of cumulative radiation duration and dose during EVAR using mobile, fixed, or fixed/3D fusion C-arms. *J Endovasc Ther*. 2016;23:944-956.
45. Weerakkody RA, Walsh SR, Cousins C, et al. Radiation exposure during endovascular aneurysm repair. *Br J Surg*. 2008;95:699-702.
46. de Ruiter QM, Moll FL, Gijsberts CM, et al. AlluraClarity radiation dose-reduction technology in the hybrid operating room during endovascular aneurysm repair. *J Endovasc Ther.* 2016;23:130-138.
47. Macchi M, Floridi C, Strocchi S, et al. Role of low dose CT angiography in the follow-up after endovascular aneurysm repair of abdominal aorta. *Acta Radiol.* 2015;56:1471-1478.
48. Nijhof WH, Baltussen EJM, Kant IM, et al. Low-dose CT angiography of the abdominal aorta and reduced contrast medium volume: assessment of image quality and radiation dose. *Clin Radiol.* 2016;71:64-73.
49. Perini P, Sediri I, Midulla M, et al. Single-centre prospective comparison between contrast-enhanced ultrasound and computed tomography angiography after EVAR. *Eur J Vasc Endovasc Surg*. 2011;42:797-802.
50. Perini P, Sediri I, Midulla M, et al. Contrast-enhanced ultrasound vs. CT angiography in fenestrated EVAR surveillance: a single-center comparison. *J Endovasc Ther*. 2012;19:648-655.

51. Guo Q, Zhao J, Huang B, et al. A systematic review of ultrasound or magnetic resonance imaging compared with computed tomography for endoleak detection and aneurysm diameter measurement after endovascular aneurysm repair. *J Endovasc Ther.* 2016;26:936-943.
52. Mell MW, Garg T, Baker LC. Under-utilization of routine ultrasound surveillance after endovascular aortic aneurysm repair. *Ann Vasc Surg*. 2017 May 10. doi:10.1016/j.avsg.2017.03.203.
53. Pontone G, Bertella E, Mushtaq S, et al. Coronary artery disease: diagnostic accuracy of CT coronary angiography-A comparison of high and standard spatial resolution scanning. *Radiology*. 2014;271:688-694.
54. Sun Z, Squelch A. Patient-specific 3D printed models of aortic aneurysm and aortic dissection. *J Med Imaging Health Informatics.* 2017;7:886-889.
55. Shi D, Liu K, Zhang X, et al. Applications of three-dimensional printing technology in the cardiovascular field. *Intern Emerg Med*. 2015;10:759-780.
56. Giannopoulos AA, Steigner ML, George E, et al. Cardiothoracic applications of 3-dimensional printing. *J Thorac Imaging*. 2016;31:253-272.

Legends

Figure 1. Phantom of a human aorta with a Zenith stent-graft placed to demonstrate stent wires (short arrows) crossing the aortic branches (long arrows). (A) Superior mesenteric artery and right renal artery ostia are crossed by 2 stent wires, and (B) the left renal artery ostium is crossed by a single stent wire. Short arrows refer to stent wires and long arrows indicate branch ostia.

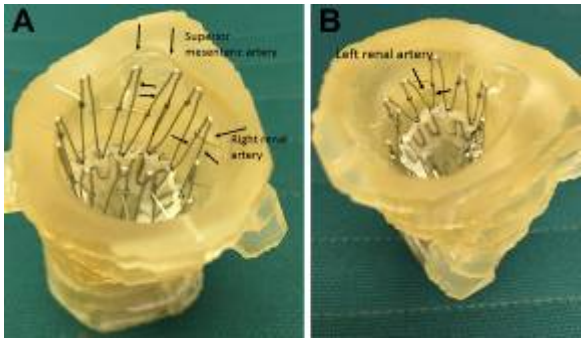

Figure 2. (A) Lateral view of a Zenith stent-graft with its uncovered suprarenal component. (B) A top view showing the hooks and barbs of the suprarenal stent wires, which are placed across the renal and visceral artery branches.

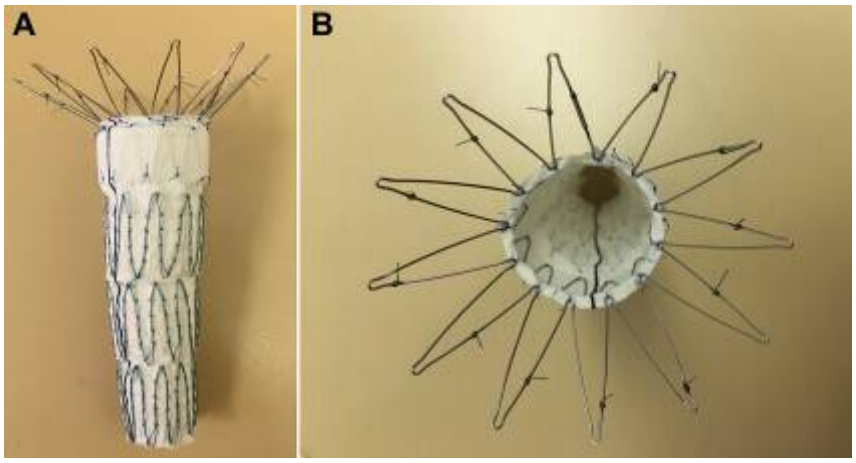

Figure 3. Synchrotron radiation virtual intravascular endoscopic images showing (A) 2 stent wires crossing the right renal ostium and (B) a single wire (long arrows) crossing the left renal ostium; image acquired using beam energy ranging from 40 to 100 keV. It is apparent that the 40-keV protocol resulted in suboptimal visualization of the stent wires due to low energy effect. The short arrows point to the hooks at the stents.

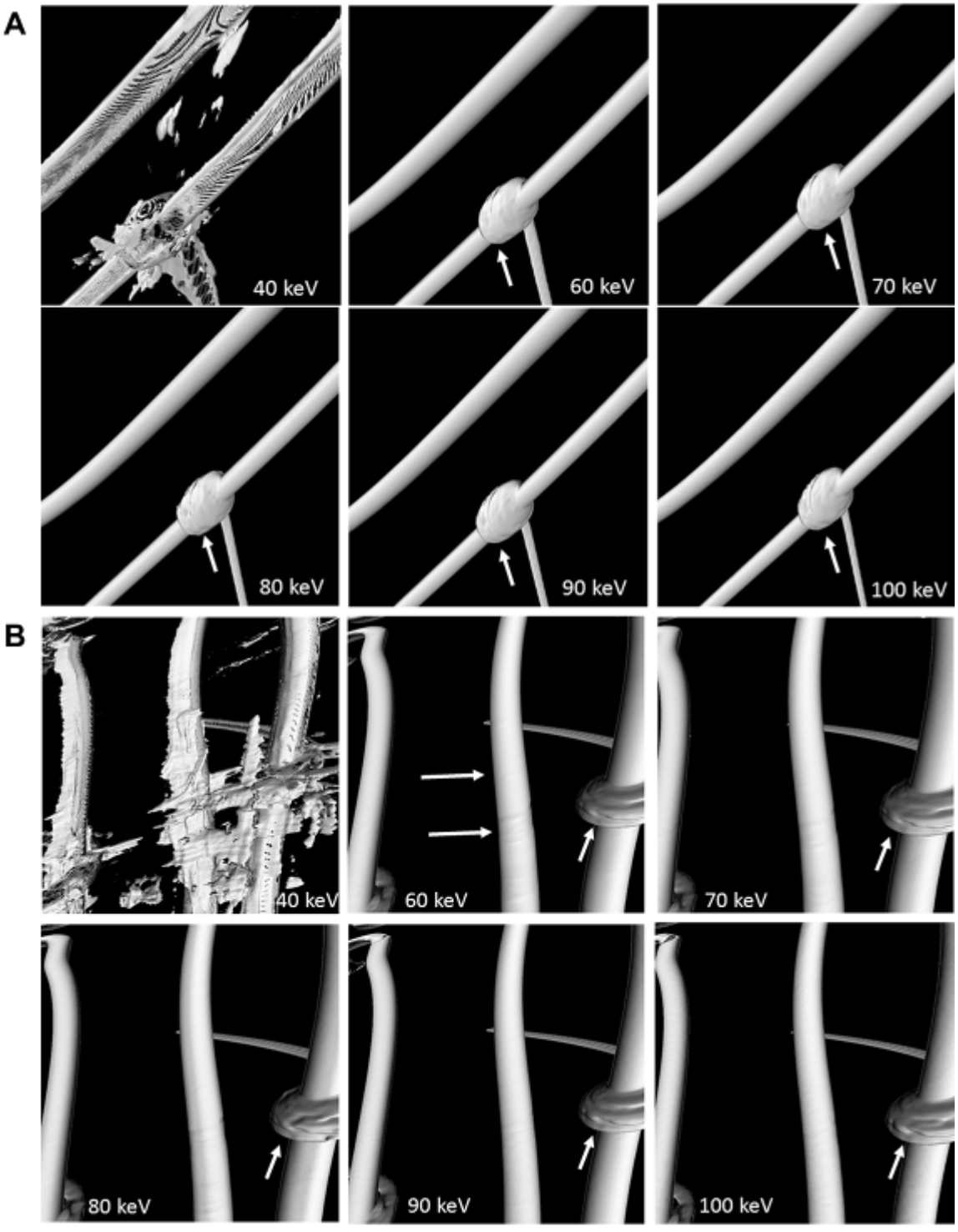

Figure 4. Computed tomography virtual intravascular endoscopy images showing (A) 2 stent wires (arrows) crossing the right renal ostium and (B) a single wire (arrows) crossing the left renal ostium; image acquired using slice thicknesses of 1.0, 1.5, and 2.0 mm.

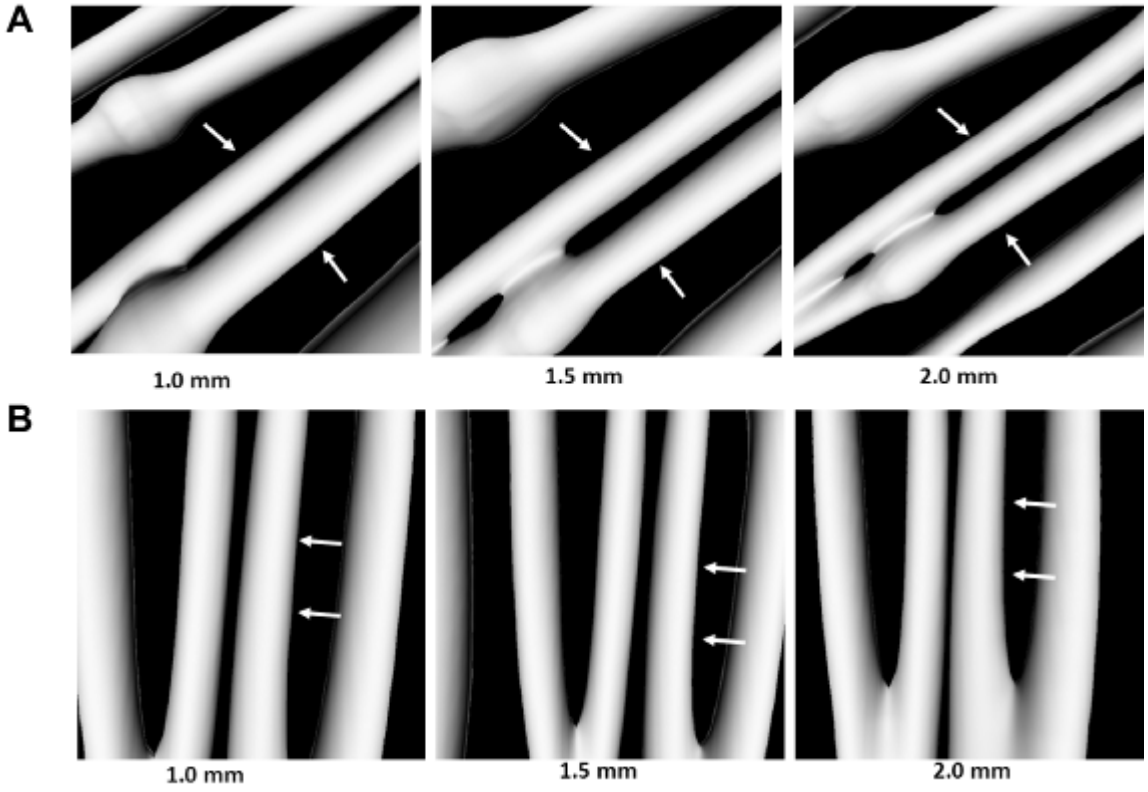

Figure 5. (A) Three-dimensional (3D) synchrotron radiation visualization of an aortic stent-graft showing the stent wires clearly, with measured wire thickness similar to the actual diameter. Arrows point to the hooks at the suprarenal stent wires. (B) 3D computed tomography (CT) images demonstrate the aortic stent-graft but with wire diameters thicker than the actual size.

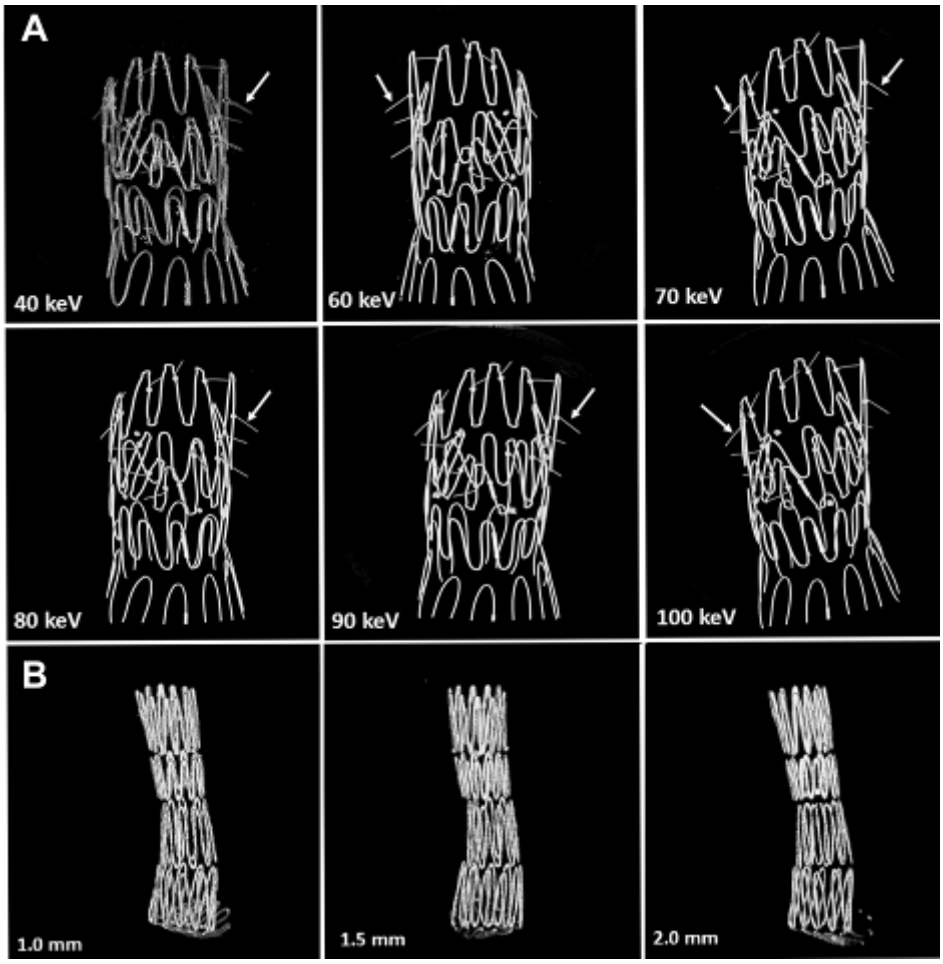

Figure 6. (A, B) Images acquired with computed tomography using a slice thickness between 0.8 and 1.0 mm in 2 patients with dissecting aneurysms treated with stent-grafts. The stent wires measured between 1.71 and 2.05 mm; the voxel size was 0.68×0.68×0.68 mm^3 and 0.78×0.78×0.78 mm^3, respectively.

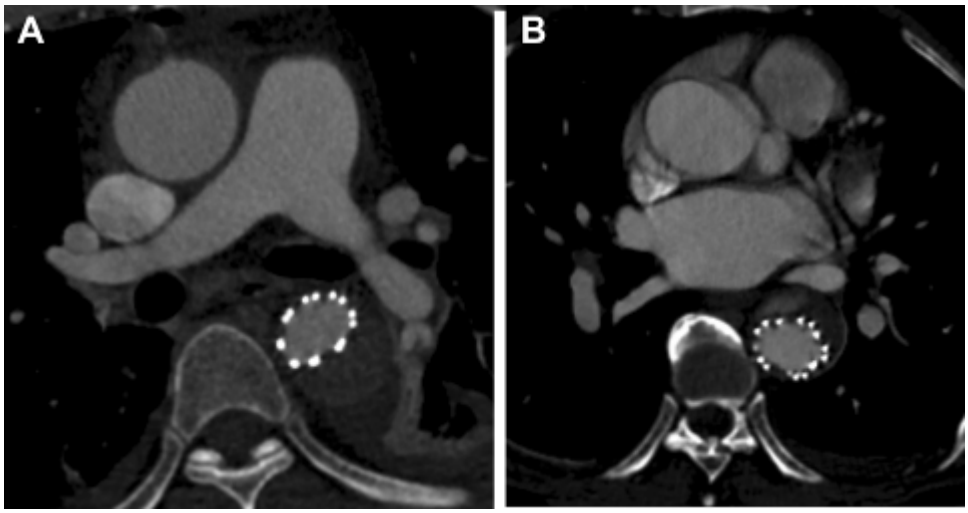

Table 1. Cross-Sectional Areas of Aortic Branch Ostia[a] Occupied by Stent Wires Measured on Images Acquired with Synchrotron Radiation.

Scanning Protocols, keV	Left Renal Ostium			Right Renal Ostium			Superior Mesenteric Artery Ostium		
	Wire Diameter *d* [b], mm	Distance *y* [c], mm	Cross-Sectional Area, %	Wire Diameters d_1, d_2, [d] mm	Distances y_1, y_2, [d] mm	Cross-Sectional Area, %	Wire Diameters d_1, d_2, [d] mm	Distances y_1, y_2,[d] mm	Cross-Sectional Area, %
40	0.48±0.01	1.19±0.01	9.98±0.34	0.51±0.01 0.53±0.03	0.98±0.04 1.13±0.01	19.62±0.42	0.48±0.02 0.51±0.01	0.59±0.03 0.77±0.02	15.86±0.51
60	0.42±0.01	1.14±0.01	9.19±0.37	0.42±0.01 0.43±0.01	0.96±0.02 1.09±0.05	17.77±0.02	0.42±0.01 0.43±0.01	0.57±0.01 0.77±0.02	13.66±0.28
70	0.40±0.02	1.21±0.01	8.56±0.34	0.41±0.01 0.43±0.02	1.00±0.03 1.12±0.01	17.43±0.84	0.41±0.01 0.52±0.01	0.52±0.02 0.75±0.02	14.94±0.41
80	0.40±0.01	1.19±0.01	8.63±0.19	0.40±0.01 0.41±0.01	0.93±0.02 1.12±0.01	16.96±0.36	0.40±0.01 0.42±0.01	0.55±0.02 0.76±0.03	13.20±0.34
90	0.38±0.01	1.21±0.01	8.37±0.12	0.38±0.01 0.39±0.01	0.96±0.02 1.09±0.02	16.17±0.12	0.39±0.01 0.40±0.01	0.53±0.01 0.78±0.02	12.72±0.41
100	0.40±0.01	1.23±0.01	8.50±0.24	0.38±0.02 0.39±0.01	0.96±0.01 1.12±0.01	16.12±0.23	0.39±0.01 0.40±0.02	0.52±0.02 0.81±0.02	12.71±0.59

[a] Diameters of the aortic branch ostia: left renal ostium 4.8 mm, right renal ostium 5.4 mm, superior mesenteric artery ostium 7.7 mm.

[b] *d* refers to the wire thickness measured on virtual intravascular endoscopy.

[c] *y* refers to the distance between the stent wire and the central axis of the branch ostium measured on virtual intravascular endoscopy.

[d] d_1, d_2 and y_1, y_2 stand for the wire thickness and distance values, respectively, corresponding to the 2 stent wires crossing the right renal and superior mesenteric artery ostia.

Table 2. Cross-Sectional Areas of Aortic Branch Ostia Occupied by Stent Wires Measured on 64-Slice Computed Tomography Images.

Scanning Protocols[a]	Left Renal Ostium			Right Renal Ostium			Superior Mesenteric Artery Ostium		
	Wire Diameter *d*,[b] mm	Distance *y*,[c] mm	Cross-Sectional Area, %	Wire Diameters d_1, d_2,[d] mm	Distances y_1, y_2,[d] mm	Cross-Sectional Area, %	Wire Diameters d_1, d_2,[d] mm	Distances y_1, y_2,[d] mm	Cross-Sectional Area, %
1.0/1.5/0.5	1.15±0.01	0.80±0.01	24.45±0.27	1.15±0.020 .37±0.02	0.70±0.01 1.10±0.06	46.92±0.94	1.37±0.01 1.57±0.02	0.80±0.01 1.20±0.03	42.69±0.49
1.5/1.5/0.75	1.22±0.02	0.89±0.01	24.47±0.27	1.22±0.01 1.33±0.01	0.74±0.02 1.37±0.02	43.66±0.94	1.40±0.01 1.57±0.01	0.80±0.02 1.30±0.01	42.66±0.33
2.0/1.5/1.0	1.22±0.01	0.80±0.01	25.49±0.27	1.22±0.01 1.37±0.02	0.89±0.01 1.0±0.01	47.93±0.70	1.28±0.02 1.51±0.03	0.83±0.01 1.27±0.02	40.40±0.91

[a]Scanning protocols are given as the slice thickness (mm)/pitch/reconstruction interval (mm). Diameters of the aortic branch ostia are the same as shown in Table 1.

[b] *d* refers to the wire thickness measured on virtual intravascular endoscopy.

[c] *y* refers to the distance between the stent wire and the central axis of the branch ostium measured on virtual intravascular endoscopy.

[d] d_1, d_2 and y_1, y_2 stand for the wire thickness and distance values, respectively, corresponding to the 2 stent wires crossing the right renal and superior mesenteric artery ostia.